# Shape of adhesive fluid controls insect adhesion in air and underwater

Pranav Sudersan,[†] Michael Kappl,[†] Thomas Endlein,[†] Bat-El Pinchasik,[‡] and Hans-Jürgen Butt[*,†]

[†]Max Planck Institute for Polymer Research, Ackermannweg 10, 55128 Mainz, Germany

[‡]Tel Aviv University, Tel Aviv-Yafo, Israel

E-mail: butt@mpip-mainz.mpg.de

Phone: +49 6131 379 111. Fax: +49 6131 379 310

## Abstract

Insects like beetles and flies can stick to various surfaces using hairy pads mediated by adhesive fluid. The pads can even attach underwater, presumably due to an air bubble trapped around the pad. There is however a lack of understanding on the exact role of the bubble for underwater adhesion. Here, we develop a simple theoretical model to estimate the net adhesion of a hairy pad due to capillary forces. We perform *in-vivo* adhesion measurements of a constrained ladybug pad as well as image its contact against smooth hydrophilic and hydrophobic substrates in air and underwater conditions. Our experiments reveal that on hydrophobic substrates, even without a bubble, the pad can show adhesion underwater comparable to that in air. Only on hydrophilic substrates, a trapped bubble is essential to generate adhesion underwater. Based on the model, this observation is explained qualitatively. Our results demonstrate that capillary forces in insects are primarily governed by the shape of the adhesive fluid and can help understand its adhesion in both air and underwater conditions.

1

# 1 Introduction

The question of how insects can walk on walls against gravity has fascinated scientific curiosity for at least the past three centuries[1,2]. We now know that animals primarily have two kinds of adhesive organs for locomotion: 1) "smooth pads" such as in ants, crickets and 2) "hairy pads" such as in flies and geckos. The hairy pad design has many advantages. They show: 1) compliance to rough surfaces due to their lower effective modulus, 2) angle dependent adhesion due to asymmetric hair geometry and 3) self-cleaning capability[3]. Many of these insects pads also secrete an adhesive fluid as seen in flies and ants[4] ("wet adhesion"), while some such as spiders and geckos rely solely on their dry hairy pads for attachment ("dry adhesion"). Under the "wet adhesion" model, fluid secretion can facilitate adhesion through surface tension and viscous forces[5], on the other hand "dry adhesion" is mediated mostly by van der Waals forces[6].

Most terrestrial beetles such as the dock beetle or ladybug have hairy pads consisting of a dense array of hair like structures called setae. The tips of each seta secrete ~1μm³of oily adhesive fluid[7], whose composition is mostly long chain n-alkanes in C-23 to C-27 range[8]. The setae have a distribution of geometries such as discoidal, spatula or pointed shaped tips depending on the pad, sex and species[9]. Single seta force measurements reveal that discoidal shaped seta show larger pull-off force than spatula and pointed setae[10], illustrating the role of hair geometry on adhesion. A recent study[11] based on an elastocapillary model has been able to reasonably predict single seta adhesion forces theoretically, confirming the dominant role of surface tension in the "wet adhesion" of beetles.

While most of the studies on beetles and other animals have focused on terrestrial conditions in air, animal attachment in underwater conditions has been relatively unexplored. Typically, underwater adhesion is complicated to achieve due to the difficulty in displacing the water layer and enable good contact[12]. Regardless, geckos show the remarkable behavior, where its shear adhesion force on hydrophobic substrates are similar in both air and underwater conditions. Interestingly, its adhesion on a fluorinated substrate is larger underwater

than in air[13]. This has been partially explained by a thermodynamic work of adhesion model assuming dry contact of hairs[14]. A study on leaf beetles[15] has also revealed that beetles can attach well to surfaces underwater. Its hairy pad traps an air bubble underwater which dewets the surface on contact. It has been hypothesized that a combination of capillary forces due the air bubble and direct contact of hairs within the dewetted zone results in attachment. However, a detailed investigation of this phenomena is lacking.

The goal of this paper is to provide a general unified picture of insect adhesion in both air and underwater conditions to substrates with different wettability. We focus our attention towards insects with hairy pads relying on a adhesive fluid for attachment. Firstly, we develop a simple theoretical model considering capillary forces to predict the net adhesion force of a hairy pad under different conditions. Secondly, we perform adhesion measurements of a single constrained pad of a live ladybug beetle in air and underwater conditions to validate our model predictions. The experiments are performed on smooth glass and fluorinated surfaces with a simultaneous observation of the contact process. Finally, we discuss key insights gained from our model and experiments as well as possible implications in understanding adhesion in other animals.

# 2    Theoretical

## 2.1    Capillary Bridge Model

We model the hairy pad system as an array of N cylindrical rods of length L and diameter, $D_h$ fixed to a flat circular base of diameter $D_p$ as shown in figure 1. For simplicity, we assume both hairs and the pad to be perfectly rigid. The tip of each cylindrical hair has a adhesive fluid of volume $V_f$ making contact with the substrate. The fluid is assumed to be pinned to the circumference of the hair and forms a capillary bridge of height d with the substrate. In order to model the contact in both air and underwater conditions, we consider three types of contacts:

1. *Air contact* - All hairs and liquid bridges are surrounded by air

2. *Underwater: Wet contact* - All hairs and liquid bridges are surrounded by water

3. *Underwater: Bubble contact* - A bubble of volume $V_b$ is trapped between the hairs. The bubble is pinned to pad circumference. Liquid bridges inside the bubble are surrounded by air while the ones outside the bubble are surrounded by water.

Let $V_f = 4/3\pi s_f^3$ and $V_b = 4/3\pi s_b^3$, where $s_f$ and $s_b$ are the radii of spheres with equivalent volumes. Fluid and bubble sizes are assumed to scale proportionally in a "self-similar" manner relative to its pinned contact size. We thus define the size parameters $\phi_f = D_f/2s_f$ and $\phi_b = D_b/2s_b$ for the fluid and bubble respectively to conveniently scale their sizes relative to the corresponding hair and pad diameters they are pinned to. The tip of the hairs are at a distance d from the the substrate.

The net adhesion force for case 1 and 2 can be calculated as:

$$F_{net} = Nf \tag{1}$$

Here, f is capillary force by a single fluid bridge at distance d, and N is the total number of hairs

For case 3, the net adhesion force is given by:

$$F_{net} = N_{inside\,bubble} f_{air} + N_{outside\,bubble} f_{water} + f_{bubble} \tag{2}$$

Here, $N_{inside\,bubble}$ and $N_{outside\,bubble}$ are the number of hairs inside and outside the bubble respectively. $f_{air}$ and $f_{water}$ are the capillary forces at distance d of a fluid bridge inside and outside the bubble surrounded by air and water respectively , and $f_{bubble}$ is the capillary force contribution due to the bubble meniscus alone. Force due to a single capillary bridge is calculated by numerical simulations, described in 2.2 and used to obtain $F_{net}$ as a function of d for each type of contact. Adhesion force of the hairy pad system is further obtained

from the minima of the respective force-distance curves.

One should note that we have considered $f_{air}$ and $f_{water}$ to be distinct terms because the capillary force by the adhesive fluid will be different in air and water due to its different contact angles and interfacial tensions. Using the Young-Dupre equations, one can derive the following relation for the contact angle of the adhesive fluid underwater:

$$\cos \theta_{fw} = \frac{\gamma_{fa} \cos \theta_{fa} - \gamma_{wa} \cos \theta_{wa}}{\gamma_{fw}} \tag{3}$$

Here, $\vartheta_{fw}$ and $\vartheta_{fa}$ are the contact angles of the adhesive fluid with the substrate in water and air respectively, $\vartheta_{wa}$ is the contact angle of water with the substrate in air, $\gamma_{fa}$ is the surface tension of adhesive fluid, $\gamma_{wa}$ is the surface tension of water and $\gamma_{fw}$ is the interfacial tension of adhesive fluid with water.

All lengths are normalized w.r.t. $s_f$ and forces are normalized w.r.t. $\gamma_{fa} s_f$.

Fixed parameter values used for all model calculations are given in 1. We consider representative hydrophilic and hydrophobic substrates with $\vartheta_{fa}$ and $\vartheta_{wa}$ values corresponding to a typical glass and fluorinated surface respectively. We assume the adhesive fluid to be an oil-lke substance and thus the interfacial tension ratios $\gamma_{wa}/\gamma_{fa}$ and $\gamma_{fw}/\gamma_{fa}$ are taken corresponding to typical values of oil and water. Area fraction of hairs relative to the pad defined as $\alpha = ND_h^2/D_p^2$, hair aspect ratio $L/D_h$ and fluid size parameter $\phi_f$ are fixed to values typical for an insect hairy pad.

Firstly, we look at how force-distance curves look like for a single pinned liquid capillary bridge. Secondly, the effect of substrate on the resultant force-distance curve of the hairy pad system is studied for each type of contact. Thirdly, the effect of varying hair size on net adhesion is studied by varying $D_p/D_h$. Finally, $\phi_b$ is varied to study the effect of bubble volume on the net underwater adhesion.

Table 1: Model parameters

| Property | Value |
|---|---|
| Area fraction, α | 0.1 |
| Hair aspect ratio, $L/D_h$ | 10 |
| Water surface tension, $\gamma_{wa}/\gamma_{fa}$ | 3 |
| Fluid-Water interfacial tension, $\gamma_{fw}/\gamma_{fa}$ | 2 |
| Fluid size parameter, $\phi_f$ | 2 |
| Hydrophilic substrate | $\theta_{fa}=6°$, $\theta_{wa}=24°$ |
| Hydrophobic substrate | $\theta_{fa}=50°$, $\theta_{wa}=120°$ |
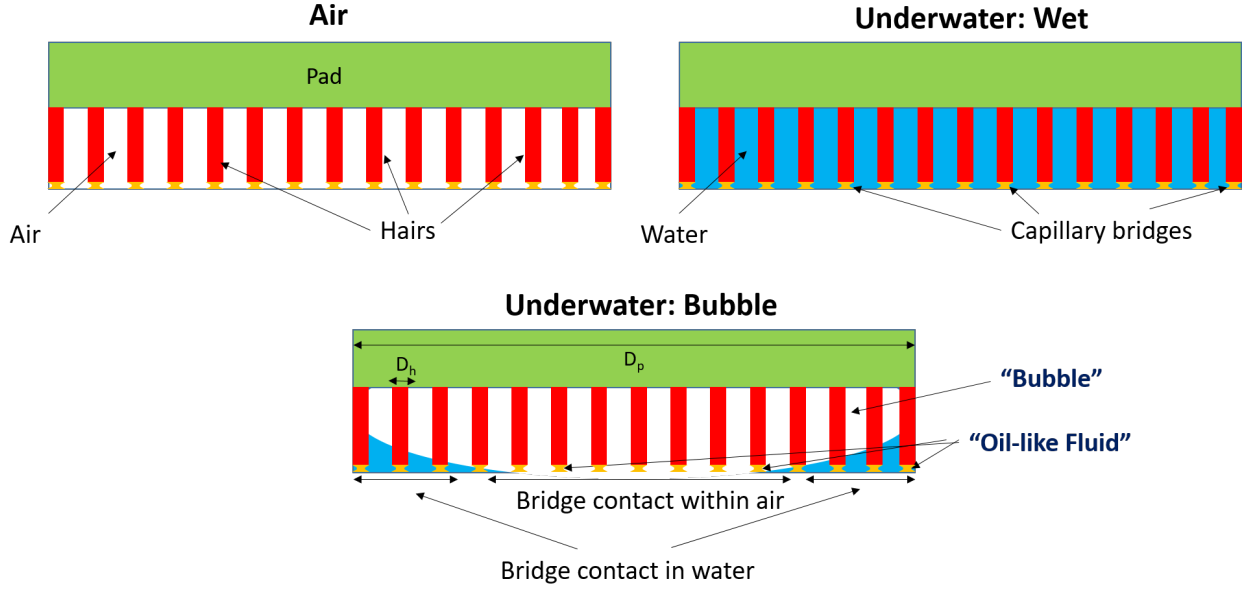


Figure 1: Capillary Bridge Model. The hairy pad system comprises of an array of rigid cylindrical hairs fixed to a cylindrical pad of diameters $D_h$ and $D_p$ respectively. Tip of each hair has an adhesive fluid forming a capillary bridge with the substrate. Hairy pad makes contact with a substrate in three ways: 1) *Air*, where the adhesive fluid bridges are surrounded by air; 2) *Underwater: Wet*, where the adhesive fluid bridges are surrounded by water; 3) *Underwater: Bubble*, where part of the adhesive fluid bridges are inside the bubble while others are outside in water. Adhesive fluid size scales with $D_h$ according to the fluid size parameter $\phi_f$. The bubble size scales with $D_p$ according to the bubble size parameter $\phi_b$. Total hair area fraction (α) and aspect ratio ($L/D_h$) are fixed. Net force is calculated from capillary contributions due to all adhesive fluid bridges and the bubble

## 2.2    Simulation Method

Capillary force due to a single adhesive fluid or bubble bridge is calculated by performing simulations in Surface Evolver[16], similar to the method described in De Souza et. al.[17]. A simple cubic geometry mimicking the liquid bridge of constant volume V is defined as the initial condition with an interfacial tension γ with the surrounding medium. The boundary conditions are set corresponding to a pinned contact line of diameter D on the top face and constant interfacial tension with the substrate on the bottom. Interfacial tension of fluid-substrate is given by γcosϑ, where ϑ is the contact angle of the fluid with the substrate. The liquid bridge spans a gap distance d between the top face and the substrate. All lengths are normalized relative to length s = $(3V/4\pi)^{1/3}$. An appropriate geometry refinement routine is chosen to evolve the liquid bridge shape to its minimum energy state. The normalized total capillary force, F=f/γs, is the sum of the laplace pressure and surface tension contributions , where:

$$f = f_{laplace} + f_{surface\,tension} = \Delta P_{laplace} A_{bottom} + 2\pi R_{bottom} \gamma \sin\theta \tag{4}$$

Here, $\Delta P_{laplace}$ which is the Laplace pressure of the equilibrium liquid bridge, $A_{bottom}$ which is the contact area of the liquid bridge with the substrate at bottom and $R_{bottom}$ which is the corresponding radius of contact are all obtained from the simulation output for an equilibrium surface.

The gap distance d is varied by fixed steps and evolved each time to obtain force-distance curves for a particular choice of D and ϑ.

For the case of a bubble bridge, the same method is followed except the contact angle is now defined as the complementary value for convenience, since $\vartheta_{wa}$ relative to water is used to characterize the substrate wettability.

## 2.3   Results

### 2.3.1   Capillary force of a pinned liquid bridge

Forces due to single pinned capillary liquid bridge in contact with a substrate are obtained via simulations (Figure2). Capillary forces are more attractive for smaller contact angles. The laplace pressure contribution to the net adhesion force dominates for contact angles less than 100° (Figure2 b). Interestingly, its contribution to adhesion force is mostly non-repulsive for contact angles greater than 90°. This is because the low volume of fluid and pinned contact line prevents the fluid bridge from having a high positive curvature due to geometric constraints . Only for a contact angle of 150° does the fluid curvature have a slightly positive curvature, manifested in its slightly repulsive laplace contribution. Surface tension makes a significant contribution to the net force only for high contact angles greater than 70°. For contact angles greater than 150°, the net force approaches zero regardless. Since laplace pressure is an indicator of the fluid bridge shape, one can make a general statement that the shape of the fluid bridge primarily determines the strength of its adhesion force for low and high contact angles. High adhesion is thus seen for contact angles less than 70° due to a net negative curvature of the fluid shape, while low adhesion is seen for contact angles greater than 150° due to its net curvature being close to zero.

The force-distance curves show a general trend of being repulsive at small distances (Figure2 a). This is a result of the pinned contact line constraint. A limited volume is available for the fluid to occupy when the gap distance is low, causing the fluid shape to bulge outward near the pinned contact line. This creates a net positive curvature, resulting in a positive laplace pressure and thus repulsion.

### 2.3.2   Capillary Bridge Model: Effect of substrate

The normalized force-distance curves for a hairy pad system on a hydrophilic and hydrophobic substrate are predicted based on Capillary Bridge Model (Figure 3). The forces for each

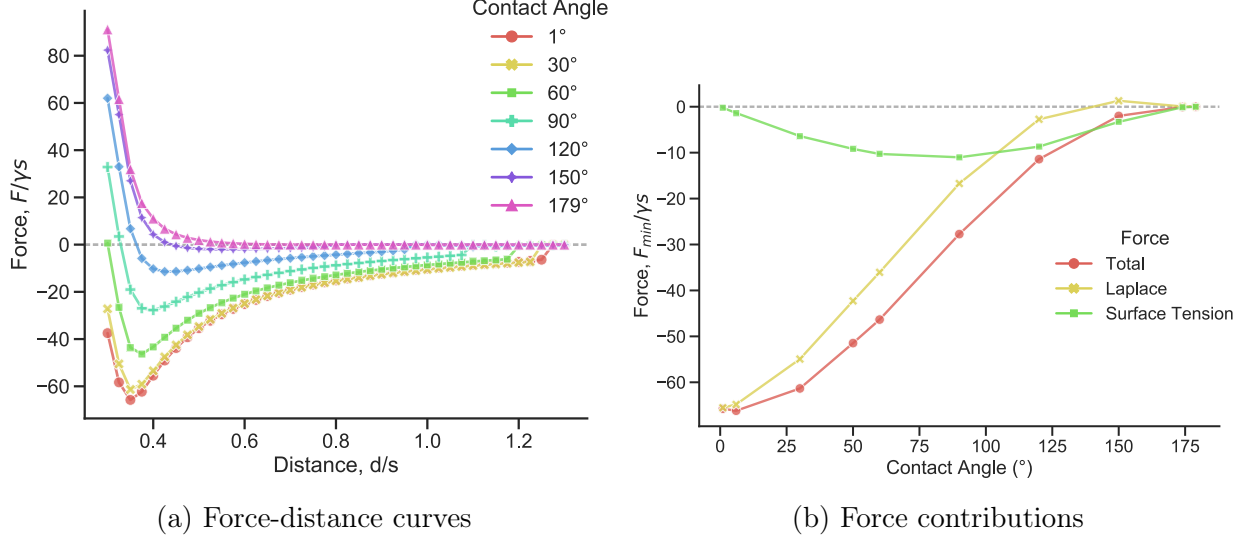(a) Force-distance curves       (b) Force contributions

Figure 2: Normalized capillary force of a single liquid meniscus in contact with a substrate below and pinned to a circular perimeter on top. Fluid size parameter $\phi_f = 2$. Negative value represents attractive force. a) Force-distance curves are shown for different contact angles of the liquid with the substrate b) Adhesion force, calculated from the minima of the corresponding force-distance curve is plotted as a function of contact angle with substrate. Laplace and surface tension contributions to the net total adhesion force are also shown.

type of contact are calculated from equations (1) and (2). Rest of the parameters are kept constant for a direct comparison of the effect of contact type and substrate chemistry.

Contact in air shows the highest attractive forces on the hydrophilic substrate. In underwater, the "wet" contact shows close to no adhesion while "bubble" contact shows moderate adhesion. In contrast, for a hydrophilic substrate, the highest attractive forces are seen in underwater "wet" contact, much larger than adhesion in air. Even underwater "bubble" contact has slightly higher adhesion than in air. Note that we have eliminated the effect of contact area by fixing the area fraction $\alpha$ 1 and pad/hair size $(D_p/D_h)$. All curves correspond to the same total hair contact area. The above effects can thus be attributed solely to how capillary force changes for each type of contact.

On a hydrophilic substrate, contact angle of the oily adhesive fluid is 6° (Table (1)) when surrounded by air and 150° when surrounded by water, as calculated from equation (3). This results in the capillary bridge shape having a net negative and slightly positive

9

curvatures respectively (Figure 9). Since laplace contribution controls capillary force at such extreme contact angles (see section 2.3.2), the fluid bridges show strong adhesion in air while underwater, it shows little to no adhesion.

On a hydrophobic substrate, the contact angles of the fluid in air and water are similarly 50° and 1° respectively. In both cases, the contact angles are low, resulting in a net attractive force in both types of contact. Additionally, the interfacial tension of the oily fluid underwater ( $\gamma_{fw}$) is twice that of in air ($\gamma_{fa}$).Thus, we see higher attractive force in an underwater "wet" contact when compared to contact in air.

The net force in the underwater "bubble" contact mainly depends on the proportion of hairs that are inside the bubble surrounded by air or outside the bubble surrounded by water (see equation (2)). For the given choice of bubble size parameter $\phi_b$, only part of the hairs are inside the bubble for the hydrophilic substrate while all the hairs are inside the bubble for the hydrophobic substrate. This is why its force curve lies in between air and underwater "wet" contact on a hydrophilic substrate, and closely follows air contact for hydrophobic substrate.

The contribution of the bubble alone to the net force in underwater "bubble" contact is negligible for both hydrophilic and hydrophobic substrates (Figure 3). Its contribution is slightly repulsive on the hydrophilic substrate due to the positive curvature of the bubble, and slightly attractive on the hydrophobic substrate due to its negative curvature. This small contribution is manifested by a small downward shift in the underwater "bubble" contact force curve on hydrophobic substrate. Here, all the hairs are trapped inside the bubble and thus its slightly higher adhesion relative to air contact is due to the small additional contribution of the bubble.

### 2.3.3 Capillary Bridge Model: Effect of hair size

The effect of changing hair or pad diameter to the net adhesion force is compared by varying the parameter $D_p/D_h$ for hydrophilic and hydrophobic substrates (Figure 4). We can
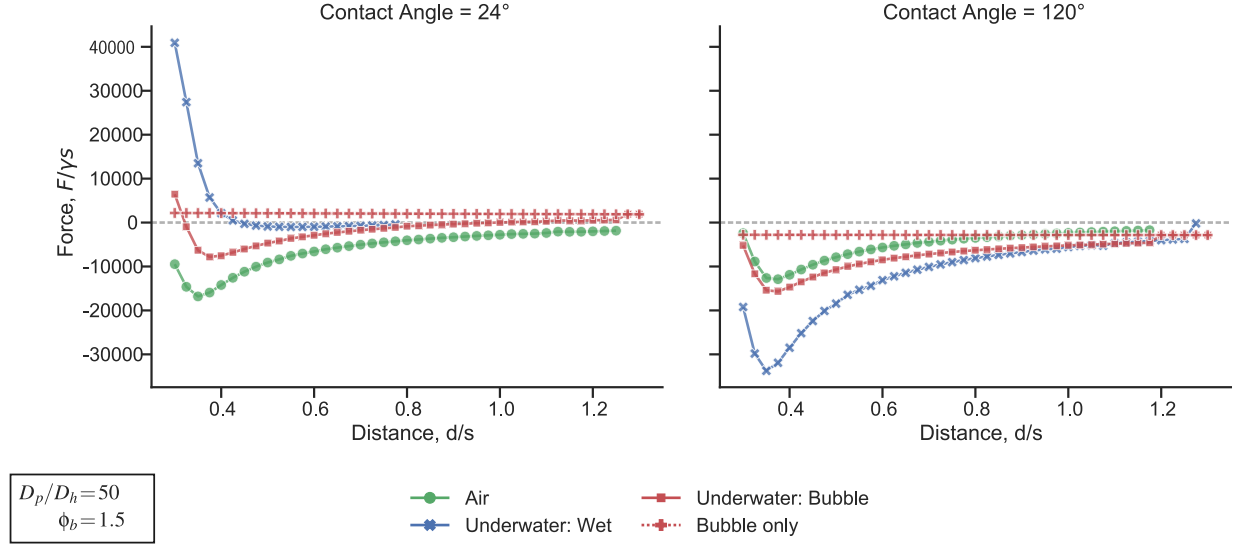
Figure 3: Theoretical force-distance curves of a hairy pad system on a hydrophilic (left) and hydrophobic (right) substrate in air and underwater conditions. Negative value represents attractive force. Normalized forces are calculated from Capillary Bridge Model, with model parameters listed in Table 1. The bubble's contribution to the net force for an "Underwater: Bubble" contact is denoted by plus symbols. Pad to hair size ratio ($D_p/D_h$) and bubble size parameter ($\phi_b$) are kept fixed

interpret Figure 4 by assuming the pad diameter $D_p$ to be fixed. Thus higher $D_p/D_h$ implies smaller hair size while keeping the total hair contact area and bubble volume constant since $\alpha$, $\phi_b$ and $D_p$ are fixed.

Adhesion force increases with decreasing $D_h$ for both hydrophilic and hydrophobic substrates in all contact types. This is consistent with the "contact splitting" theory which predicts higher adhesion on splitting contacts to smaller size[18]. Since $\phi_f=2$, the size of the adhesive fluid scales in a self-similar manner relative to the size of the hair. Thus, the total force scales proportional to the number of contacts N and adhesion force increases as $D_h$ is decreased.

Similar to the trend in Figure 3, contact in air shows the highest adhesion force for the hydrophilic substrate for all hair sizes, while on the hydrophobic substrate, underwater "wet" contact shows highest adhesion. Underwater "bubble" contact shows intermediate adhesion between air and underwater "wet" contact types.

The bubble only contribution to underwater "bubble" contact gets repulsive as hair size

11

is decreased for both substrates (Figure 4). Since the aspect ratio $L/D_h$ is fixed (Table 1), decreasing the hair size also decreases its length. The bubble has less space available between the pad and the substrate, resulting in it bulging outwards near the pinned contact line on top. Thus, bubble contribution gets repulsive as hair size decreases.
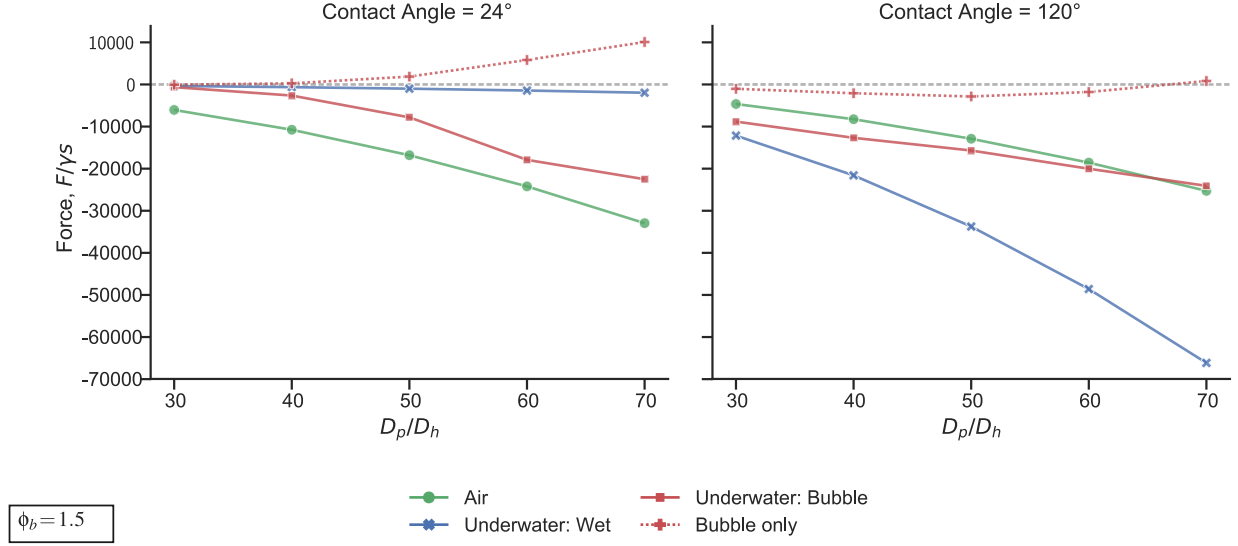


Figure 4: Normalized adhesion force of hairy pad system on a hydrophilic (left) and hydrophobic (right) substrate as a function of pad to hair size ratio ($D_p/D_h$), calculated from Capillary Bridge Model. Negative value represents attractive force. The bubble's contribution to the net force for an "Underwater: Bubble" contact is denoted by plus symbols. Bubble size parameter ($\phi_b$) is kept fixed. Adhesion forces are calculated from minima of the respective force-distance curves.

### 2.3.4 Capillary Bridge Model: Effect of bubble volume

The effect of varying bubble size parameter $\phi_b$ on the net adhesion force of the underwater "bubble" contact for hydrophilic and hydrophobic substrates are compared (Figure 5). Increasing $\phi_b$ implies smaller bubble volume and thus larger proportion of fluid bridges outside the bubble. From section 2.3.2, we know that on the hydrophilic substrate, fluid bridges outside the bubble contributes to very little adhesion due to its positive curvature. Thus, decreasing the bubble volume decreases adhesion force due to the larger proportion of hairs outside the bubble. In contrast, on the hydrophobic substrate, fluid bridges outside the bubble has a stronger contribution to the net capillary force due to the low contact angle and

12

high interfacial tension in water. Thus, adhesion force increases for a hydrophobic substrate as bubble size decreases.

Bubble's contribution to the net adhesion force is small regardless of its size. We see that a smaller bubble (large $\phi_b$) tends towards more attraction by the bubble in both kind of substrates, though negligible. For small values of $\phi_b$, the net underwater "bubble" contact force mostly follows the "bubble only" contribution, because the bubble in this case is big enough to entrap all hairs inside it. Thus initially, the force contribution due to fluid bridges remain same while the bubble contribution increases slightly as $\phi_b$ increases. Once the bubble gets small enough and part of the fluid bridges make contact outside the bubble, the force trend changes with a steep decrease or increase in adhesion force on hydrophilic and hydrophobic substrates respectively.

To summarize, on a hydrophilic substrate, bubble can promote adhesion by being large enough to keep the adhesive fluid bridges inside the bubble. This is because "wet" hairs underwater show no adhesion and the only way to achieve adhesion is by maintaining the hairs in air environment. On a hydrophobic substrate however, a smaller or no bubble is preferred, as the bubble has little effect on improving adhesion force. This is because hairs making a "wet" contact underwater shows stronger adhesion than in air due to the fluid's smaller contact angle and higher interfacial tension. In either case, the bubble by itself hardly contributes to the net force. Despite its large size, the bubble fails to overcome the combined contribution of the much smaller fluid bridges to the total force

# 3 Experimental

In order to validate the predictions from the Capillary Bridge Model, we perform normal adhesion force measurements on a constrained pad of a live ladybug beetle. We characterize adhesion by the pull-force during detachment. Measurements are performed against smooth glass and fluorinated surface to represent hydrophilic and hydrophobic substrates respec-
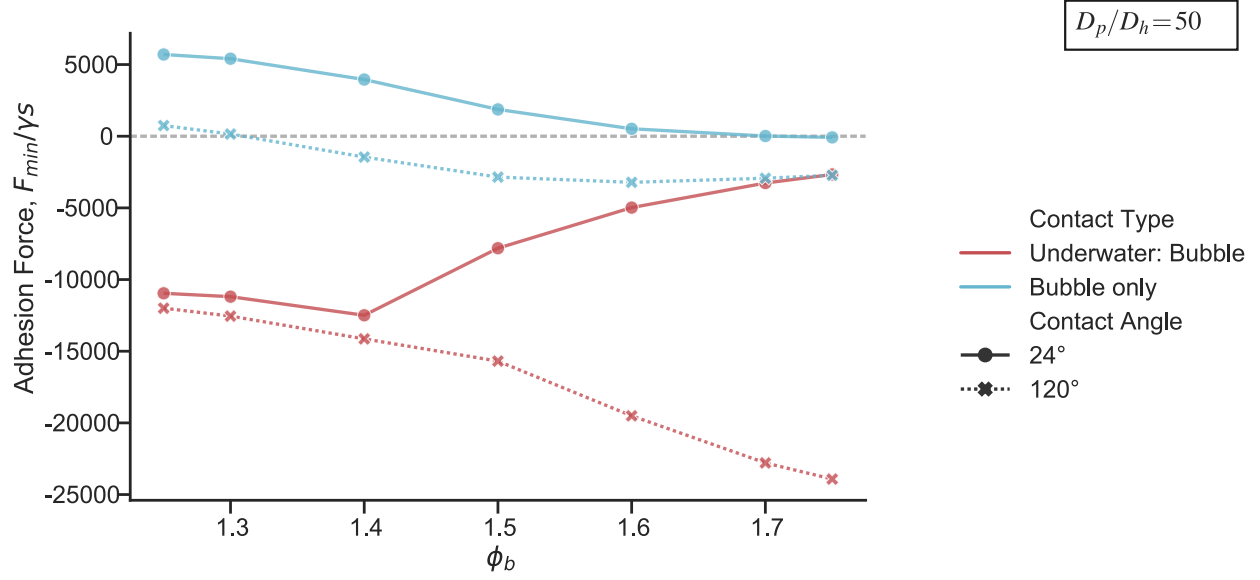
Figure 5: Normalized adhesion force of hairy pad system as a function of bubble size parameter ($\phi_b$) for "Underwater: Bubble" contact type (red). Negative value represents attractive force. Higher $\phi_b$ value implies a smaller bubble size. Bubble's contribution to the net adhesion is shown in blue. Here, pad to hair size ratio ($D_p/D_h$) is kept fixed. Adhesion forces are calculated from minima of the respective force-distance curves.

tively. The three possible contact types: Air, Underwater "Wet" and Underwater "Bubble" are studied for each substrate

## 3.1 Material and Methods

### 3.1.1 Substrate preparation

Standard 20 mm glass coverslips are used as the hydrophilic substrate. Glass was wiped with Isopropanol, rinsed in water and dried under nitrogen jet. The surface was then plasma cleaned in oxygen plasma chamber (Diener Electronic Femto) for 10 mins at120 W power. The surface was further rinsed with water and dried under nitrogen jet.

For the hydrophobic substrate, glass cover slip was coated with a fluorosilane via chemical vapor deposition (CVD) method. Glass was first cleaned using IPA and plasma treated as before. 0.2 ml of Trichloro(1H,1H,2H,2H-perfluorooctyl) silane (PFOTS), procured from Sigma Aldrich, was put in a sealed chamber along with the the glass cover slip. The chamber

was placed under 100 mbar pressure for 10 mins as it undergoes CVD. Glass substrates was finally annealed at 150℃ for 3 hours.

The substrate wettability was characterized by dynamic contact angle measurements performed in DataPhysics OCA 35 contact angle goniometer using water and n-hexadecane. "Needle in drop" method was used to measure the advancing and receding contact angles for a maximum drop volume 10 μl and 0.5 μl/s flow rate. Static contact angles were measured for a 5 μl drop.

Table 2: Static and dynamic contact angles measurements

| Substrate | Liquid | $\theta_A$ | $\theta_R$ | $\theta_S$ |
|-----------|--------|------------|------------|------------|
| Glass | Water | 60±3° | 21±2° | 24±1° |
| | n-Hexadecane | <10° | <10° | <10° |
| PFOTS | Water | 122±1° | 93±1° | 110±2° |
| | n-Hexadecane | 86±1° | 50±2° | 70±1° |

### 3.1.2 Field desorption mass spectroscopy

*############## inputs from Bat-El ##############*

- Backleg of an Asian Ladybird cut immediately after death

- Leg immeresed in 100 μl water for 15 minutes. Immersed in THF for 20 mins

- Control sample leg only immersed in THF for 20 mins

### 3.1.3 Specimen preparation

Seven-spotted adult ladybug beetles (*Coccinella Septumpuctata*) procured from Katz Biotech were used for adhesion tests. The beetles were maintained in a plastic box filled with leaves, twigs and stones under room conditions with access to sunlight to give it a close to natural habitat. The beetles were fed with raisins and honey.

Experiments were done only on male beetles. For the test, the beetle's leg was constrained similar to the method described by Bullock et al[9]. The steel ball fixed with a piece of thick

solder wire was used as a holder to fix and constrain the beetle and its leg. The beetle was first anesthetized using dry ice and glued to the steel ball on its back. Its front left leg was carefully stuck to the solder wire using Blue-Tac. Its claw was fixed using epoxy glue to prevent any wiggling. The leg was aligned such that only the distal pad of its leg can make contact. Teflon tape was used like a blanket to wrap around the rest of its body to prevent interference by its other legs.

After measurements, the beetle was carefully removed without hurting it and set free to ponder about that confusing experience.

### 3.1.4 Adhesion test

Adhesion measurements were performed on a custom force measurement setup developed in-house (Figure 6 a). A fiber optic displacement sensor (Philtec D20) together with a steel bending beam constitutes the vertical force sensor. Beam deflection was calibrated using 4 known weights to get the corresponding force. A plastic 3D printed substrate holder was glued to the end of the bending beam. The holder was designed to allow switching from one substrate to another without removing any glue. It's "tank" like design also allows it to be filled with water for underwater tests. The sensor was mounted on a stage consisting of a piezo used for lateral motion, XYZ motors and goniometer for substrate alignment. Additionally, a separate piezo fixed to the frame is used for vertical up-down motion, bringing the specimen in contact with the substrate from top. A XYZ micro-manipulator together with a free stainless steel ball allows controlling the specimen alignment in any direction. A coaxial illuminated tube microscope (Navitar) with 2x objective and a stereo-microscope with 1x objective (Wild Heerbrugg) fit with cameras are used to record the sample contact with the substrate from bottom and side views respectively. The data acquisition from the force sensor and cameras together with an appropriate piezo motion steps are synchronized using a custom LABVIEW program. Force data was acquired at a sample rate of 984 Hz, averaged to 512 points per motion step. Videos were recorded at 20 frames per second.

The vertical and lateral piezos were together used to perform approach-retract adhesion tests with the substrate to get the pull-off force. However, instead of a simple down-up motion some additional motion steps were included (Figure 6 b). A 100 μm lateral slide motion was done after initial approach step to better orient the hairs with the substrate[9]. An additional 10 μm compression step (approach) was done to ensure all hairs are loaded and makes good contact with the surface. A 1 second "Pause" step was done to eliminate any viscoelastic effects before finally retracting the leg away from the substrate. All approach, retract and sliding motion was done at a speed of 62.5 μm/s. Bottom view video recordings were used for contact area extraction while the side view imaging is used only to visually aid orienting the pad with the substrate before a test. Figure 6 b shows a typical measurement data where recorded force is plotted as a function of time along with the observed pad contact area extracted via image processing.

For underwater experiments, 1 ml of deionized water was poured into the substrate holder. In order to achieve an underwater "wet" contact, the likelihood of bubble trapping between the pad was reduced by degassing the water in a vacuum chamber for 3 hours before use.

10 contact measurements were done on the same spot of the surface to equilibriate the pad system. 5 measurements were subsequently performed on a fresh spot of the substrate for each type of contact and is used for data analysis. Experiments were repeated with 5 distinct beetles for each type of contact. In total, 30 beetles were tested.

### 3.1.5    Data analysis

Extraction of pull-off force from force data, image processing, plotting and statistical analysis are all performed in "*Buggee*"[19], a tool written in Python using open-source libraries for synchronous analysis of force data and video recordings.

For measurements in air, pull-off force is defined as the minimum force during the final retraction step. For underwater measurements, an additional correction needs to be done first. During the piezo motion, contact line of the immersed holder at water surface changes,
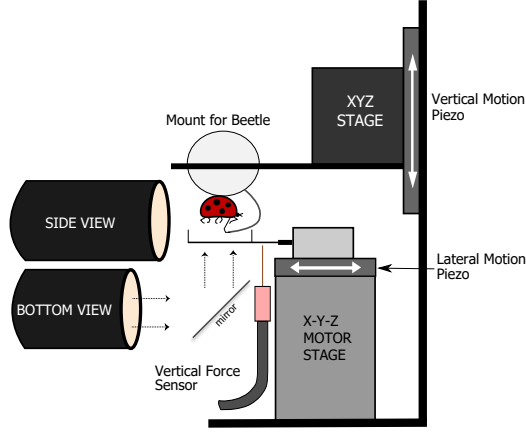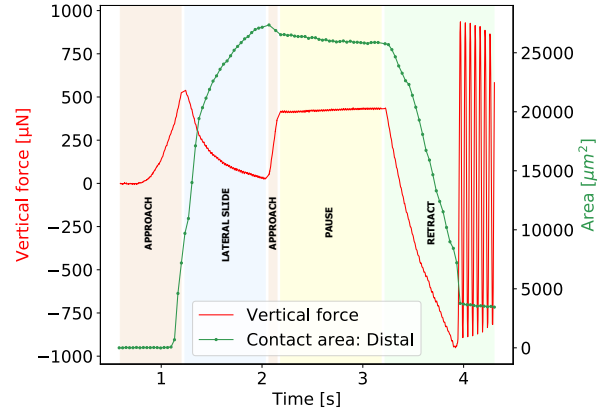
Figure 6: a) Adhesion test setup b) Representative force data and contact area of distal pad for a typical measurement. Shaded regions represent distinct motion steps. Minimum peak value during final retract step is taken as adhesion force.

influencing the force readout due to surface tension. This effect needs to be canceled. So, a background force data is recorded where the submerged beetle makes no contact with the substrate. The background forces is then subtracted from a typical force data with substrate contact to correct for the external surface tension effects. After this, the pull-off force is calculated from the minima as before.

Data sets are compared for statistical deviations using pairwise Tukey t-test and their corresponding effect sizes are compared using Pearson correlation coefficients. Shapiro-Wilk test was done for each data sets to verify normal distribution of its residuals and Levene's test was done to check equality of the respective variances, thus validating the assumptions involved in the Tukey test.
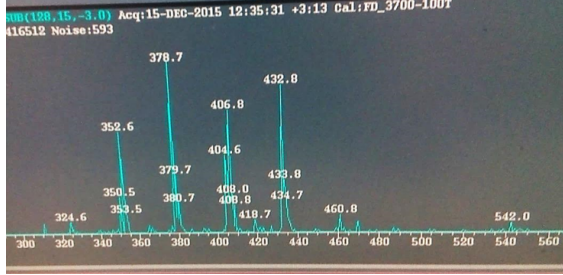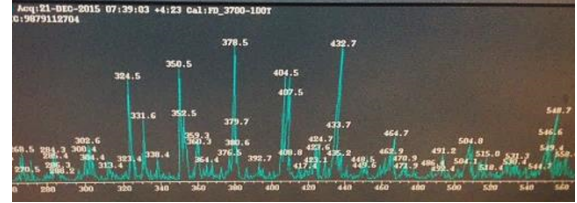
## 3.2 Results

### 3.2.1 Field desorption mass spectroscopy

*############## inputs from Bat-El ##############*

- Adhesive fluid composition is mostly n-alkanes/hydrocarbons? (How?)

- Fluid composition doesn't change after washing with water (Figure )

- Adhesive fluid remains intact to hair tips underwater



(a) Without rinsing in water

(b) After rinsing in water

Figure 7: Field desoption mass spectroscopy data of adhesive fluid extracted from Asian ladybug beetle #### *Inputs from Bat-El* ####

### 3.2.2 Adhesion test

Adhesion force for the distal pad of ladybug beetle against glass and PFOTS in air and underwater conditions are compared (Figure 8). In air, there is only a small difference in the median adhesion force on glass and PFOTS. The small difference can be attributed to the higher receding contact angle of oil in PFOTS when compared to glass (Table 2). In underwater, a huge difference is seen in the forces between glass and PFOTS for a wet contact. On glass, very small adhesion is recorded while PFOTS shows an adhesion close to that in air. For a bubble contact, both glass and PFOTS show similar adhesion. Statistical significance values for comparison of the different contact types (Table 3) support the above conclusions.

Apart from the three predicted contact types, we also observed an additional fourth contact type which randomly occurs underwater, labeled as "bad contact". During such a contact, the bottom view contact area recordings don't show a prefect contact of hairs with the substrate as is usually seen for the other three contact types. "Bad contact" always shows no adhesion with either glass or PFOTS substrate. While it's not completely clear why such a contact occurs, there can be two possible reasons:

1. The hairs could get bundled due to a small air meniscus inside the hairs, resulting in its disorientation.

2. The substrate is not dewetted during contact, causing a thin water layer on the surface to prevent adhesion.
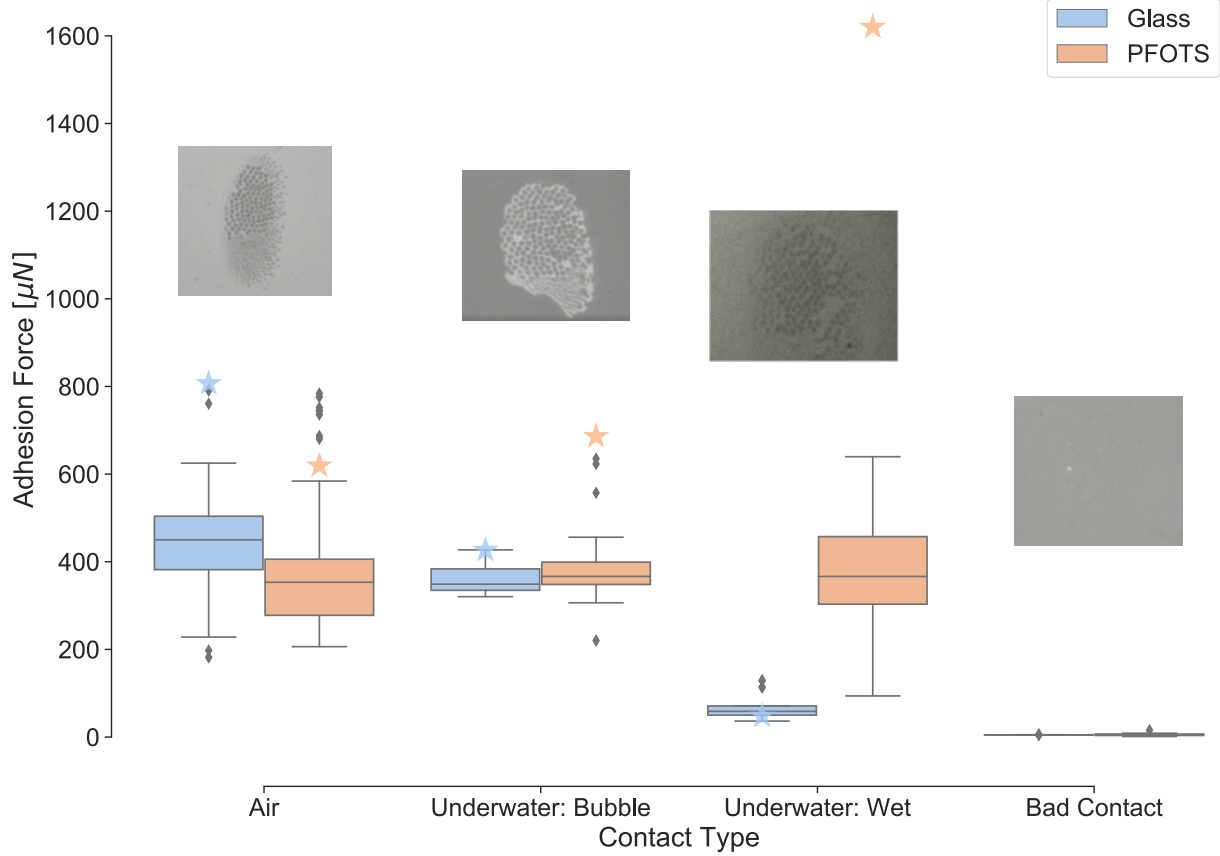


Figure 8: Adhesion force measurements of ladybug beetle on glass and PFOTS substrates in air and underwater conditions. Values represent peak force of a distal pad pulled off from each substrate at 62.5 μm/s retraction speed. Three types of contact are seen in underwater experiments and are represented separately: "Bubble", "Wet" and "Bad Contact". Insets show bottom view images of the corresponding contact types. Stars represent theoretical predictions of adhesion force calculated from Capillary Bridge Model, where hair diameter = 4 μm, pad diameter = 200 μm, hair height = 40 μm, number of hairs = 500, fluid size parameter $\phi_f = 2$ and bubble size parameter $\phi_b = 1.5$.

Table 3: Statistical analysis of adhesion force. p-value and T are obtained from pair-wise Tukey test between A and B while keeping the third parameter fixed. r values represent the corresponding Pearson correlation coefficient

| A | B | Fixed | p-tukey | T | r |
|---|---|---|---|---|---|
| Air | Underwater: Bubble | Glass | 0.211 | 1.95 | 0.298 |
| Air | Underwater: Wet | Glass | 0.001 | 10.985 | 0.846 |
| Underwater: Bubble | Underwater: Wet | Glass | 0.001 | 5.857 | 0.774 |
| Air | Underwater: Bubble | PFOTS | 0.9 | 0.017 | 0.002 |
| Air | Underwater: Wet | PFOTS | 0.854 | 0.767 | 0.085 |
| Underwater: Bubble | Underwater: Wet | PFOTS | 0.9 | 0.561 | 0.083 |
| Glass | PFOTS | Air | 0.16 | 1.405 | 0.151 |
| Glass | PFOTS | Underwater: Bubble | 0.348 | -0.939 | -0.192 |
| Glass | PFOTS | Underwater: Wet | 0.001 | -8.258 | -0.776 |

# 4 Discussion

Our experiments demonstrate for the first time that the ladybug beetle can attach to a hydrophobic substrate even without a bubble trapped around its hairs. A previous study [15] had hypothesized that bubble is necessary for underwater attachment in beetles. This is however only true for glass substrates where only the underwater "bubble" contact shows adhesion while "wet" contact shows poor adhesion. For a hydrophobic substrate, all forces lie in a similar range regardless of the type of contact, with the only exception of "bad contact".

Experimental results are in qualitative agreement with the predictions from Capillary Bridge Model (Figure 8). Here, we set the model parameters to resemble a ladybug's distal pad. On PFOTS, "wet" contact shows adhesion similar to that in air, while on glass, "wet" contact has very low adhesion. This is explained by the different oil contact angles and interfacial tension for these two substrates in air and underwater conditions (Figure 9). The measurements however don't show a significantly higher adhesion for the underwater "wet" contact on PFOTS when compared to its adhesion in air as predicted by the model. This could be due to the additional complexity involved in making a good underwater contact. We already observe that "bad contact" can lead to complete loss of adhesion. It is thus

possible that such bad contacts are happening locally for some hairs which reduces the net adhesion force for the "wet contact".

The role of bubble for underwater adhesion is further clarified based on the model. The bubble by itself has a negligible capillary contribution to the net adhesion force underwater. Bubble can only help in adhesion on a hydrophilic substrate by providing the hairs an air environment such that the liquid capillary bridges show adhesion similar to that in air. For a hydrophobic substrate, having a trapped bubble has no significant effect on improving adhesion as even a "wet" contact underwater shows adhesion similar to that in air.

The model assumes a perfect contact of each hair which detaches simultaneously to give a theoretical maximum adhesion force achievable. Our experimental conditions are however far from such assumptions. The pad always makes a partial contact with the substrate at a random angle, which is difficult to precisely control. During detachment, the pad typically peels of from its proximal to distal end unlike a simultaneous detachment. Our model also assumes the hairs to be perfectly rigid and of similar geometry unlike reality. Thus it's not surprising that the model overestimates the adhesion forces. The predictions are however in the same order of magnitude as experiments, and the qualitative trend is consistent for both hydrophilic and hydrophobic substrates in air and underwater.

Our study provides further validation that capillary forces by the adhesive fluid controls insect adhesion and van der Waals contribution, if any, must be negligible. For underwater "wet" contact, the pad adheres strongly to a PFOTS substrate, but poorly to a glass substrate even though it shows similarly strong adhesion to both substrates in air. This behavior can only be explained by capillary forces.

Our findings can also be extended to other animals relying on oily adhesive fluid for adhesion. Ants for example show similar adhesion on hydrophobic substrates under wet and dry conditions[20], similar to what we see in a ladybug. Recent adhesion experiments on geckos reveal that it can attach well to fluoropolymer substrates underwater while shows little adhesion to the same substrate in air[13,14]. Although a work of adhesion model assuming dry
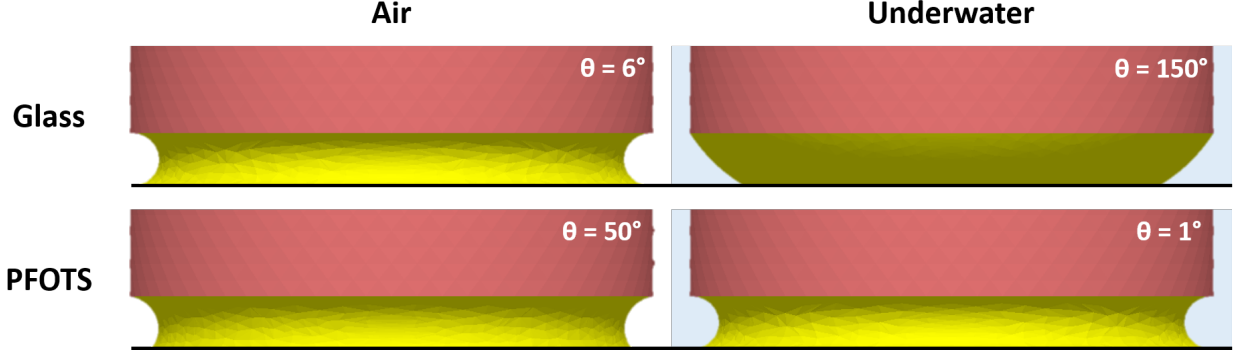
Figure 9: Simulation snapshots of oil capillary meniscus in contact with glass and PFOTS in air and underwater conditions

contact was able to explain this result qualitatively, the same model fails to predict the low underwater adhesion seen for the slightly hydrophilic substrates such as PMMA or PET. Geckos are thought to rely on van der Waals forces via dry contact with the substrate[6], although recent observations of phospholipid footprints left behind walking geckos[21] could change that picture. Since geckos adhere poorly to PTFE (surface energy ~ 20 mN/m) one can speculate that the phospholipid material has a higher surface energy, and consequently makes a higher contact angle with PTFE in air. Let us assume the phosopholipid material to be a fluid similar to oil with $\gamma_{fa}$=30 mN/m and $\gamma_{fw}$= 42 mN/m. such that its contact angle with PTFE is 80°. Equation 3 then gives us an underwater contact angle of 70° for the phospholipid fluid. Thus, the Capillary Bridge Model can predict a higher adhesion underwater than in air with PTFE due to its lower contact angle and higher interfacial energy underwater. Based on similar assumptions, we predict the net adhesion force for a gecko on different substrates (Figure 10). The adhesion force predictions are in qualitative agreement with the whole animal experimental shear force values reported for the gecko, with the trend of higher adhesion in air than underwater for glass, similar adhesion in air and underwater for PMMA/OTS-SAM and lower adhesion in air than underwater for PTFE. We thus propose that the underwater experiments performed on geckos[13,14] is an indirect proof of capillary contribution to gecko adhesion.. We suggest performing single seta adhesion force tests similar to Autumn et. al.[6] using a hydrophilic and fluorinated probe in air and

underwater conditions to validate the role of capillary contributions to gecko adhesion.

We have so far limited our analysis to only smooth substrates. Insects in the real world however interacts with rough substrates all the time. Previous studies[22] have shown that substrate roughness is a more dominant parameter than substrate chemistry in controlling insect adhesion. Future work will explore how roughness can impact the net capillary force as predicted by our model. Our study can have potential applications in the design of bioinspired materials to achieve adhesion via capillary bridges. Bubble can be possibly be used to control underwater adhesion by changing the relative proportion of the arrays inside and outside the bubble. A suitable choice of adhesive fluid can be made tailored to the substrate and environment of application for optimal adhesion performance.
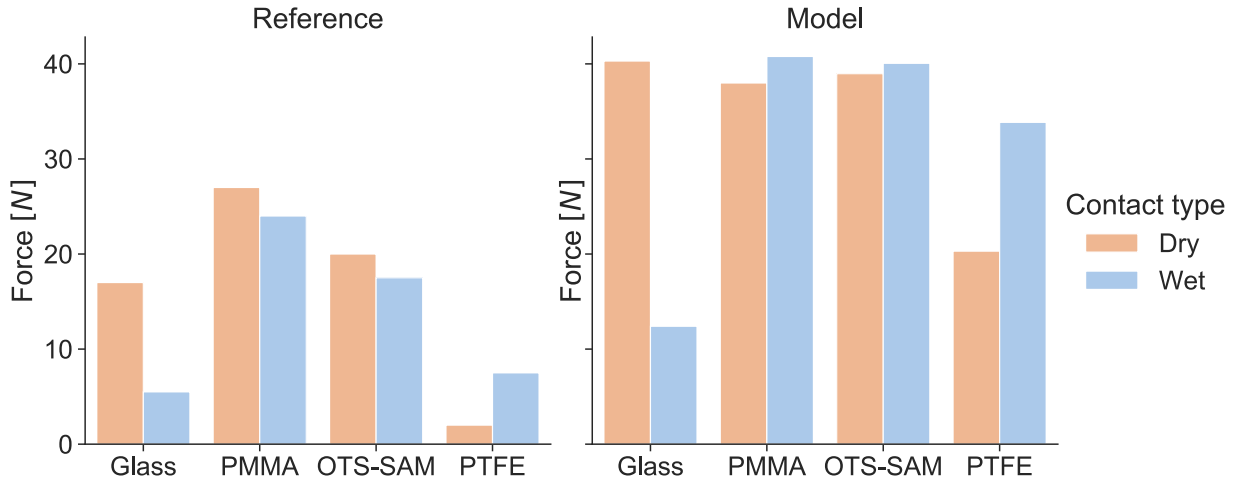


Figure 10: Whole animal adhesion force of gecko on various substrates. Experimental shear adhesion values are reproduced from Stark et. al.[13]. Normal adhesion forces for each gecko toe are theoretically estimated from Capillary Bridge Model, with hair diameter = 400 nm, toe diameter = 4 mm, fluid size parameter $\phi_f = 2$ and 10% hair coverage. "Underwater:Wet" contact is assumed for "Wet" contact. Net adhesion force is calculated by assuming 5 toes on each leg and 4 legs in total on a gecko. Interfacial tension of phospholipid layer (PL) in air and water are assumed to be 30 mN/m and 42 mN/m respectively. PL contact angles with glass, PMMA, OTS-SAM and PTFE are assumed to be 6°, 10°, 20° and 80° respectively. The corresponding water contact angles are 50°, 85°, 94° and 97° respectively, as reported in Stark et. al.[13].

# 5 Conclusions

1. Capillary force due to the oily fluid secretion of an insect is primarily responsible for its adhesion to various smooth substrates both in air and underwater conditions. Laplace pressure contribution, manifested in the adhesive fluid shape, dominates the net adhesion contribution.

2. Contact angle and interfacial tension of adhesive fluid changes depending on the surrounding medium and substrate in contact. This explains the insect's strong adhesion on a hydrophobic substrate and weak adhesion on a hydrophilic substrate when its hairs are completely wet.

3. In underwater, bubble trapped by the adhesive pad has negligible capillary contribution to the total force. Trapped bubble promotes adhesion only on a hydrophilic substrate by providing an air medium to the adhesive fluid bridges inside it in contact with the substrate.

4. Future studies on insect adhesion should characterize oleophilicity rather than hydrophilicity of a substrate, since oil contact angle primarily controls its adhesion to the substrate.

# 6 Acknowledgement

# References

(1) Hooke, R. *Micrographia, or, Some physiological descriptions of minute bodies made by magnifying glasses : with observations and inquiries thereupon*; The Royal Society,

1665.

(2) Stork, N. E. Experimental Analysis of Adhesion of Chrysolina Polita (Chrysomelidae: Coleoptera) on a Variety of Surfaces. *The Journal of Experimental Biology* **1980**, *88*, 91.

(3) Federle, W. Why are so many adhesive pads hairy? *J Exp Biol* **2006**, *209*, 2611–21, DOI: 10.1242/jeb.02323.

(4) Federle, W.; Riehle, M.; Curtis, A. S.; Full, R. J. An Integrative Study of Insect Adhesion: Mechanics and Wet Adhesion of Pretarsal Pads in Ants. *Integrative and Comparative Biology* **2002**, *42*, 1100–1106, DOI: 10.1093/icb/42.6.1100.

(5) Dirks, J. H. Physical principles of fluid-mediated insect attachment - Shouldn't insects slip? *Beilstein J Nanotechnol* **2014**, *5*, 1160–6, DOI: 10.3762/bjnano.5.127.

(6) Autumn, K.; Sitti, M.; Liang, Y. A.; Peattie, A. M.; Hansen, W. R.; Sponberg, S.; Kenny, T. W.; Fearing, R.; Israelachvili, J. N.; Full, R. J. Evidence for van der Waals adhesion in gecko setae. *Proceedings of the National Academy of Sciences* **2002**, *99*, 12252, DOI: 10.1073/pnas.192252799.

(7) Peisker, H.; Gorb, S. N. Evaporation dynamics of tarsal liquid footprints in flies (Calliphora vicina)and beetles (Coccinella septempunctata). *The Journal of Experimental Biology* **2012**, *215*, 1266–1271, DOI: 10.1242/jeb.065722.

(8) Geiselhardt, S. F.; Geiselhardt, S.; Peschke, K. Comparison of tarsal and cuticular chemistry in the leaf beetle Gastrophysa viridula (Coleoptera: Chrysomelidae) and an evaluation of solid-phase microextraction and solvent extraction techniques. *Chemoecology* **2009**, *19*, 185, DOI: 10.1007/s00049-009-0021-y.

(9) Bullock, J. M.; Federle, W. Division of labour and sex differences between fibrillar,

tarsal adhesive pads in beetles: effective elastic modulus and attachment performance. *J Exp Biol* **2009**, *212*, 1876–88, DOI: `10.1242/jeb.030551`.

(10) Bullock, J. M.; Federle, W. Beetle adhesive hairs differ in stiffness and stickiness: in vivo adhesion measurements on individual setae. *Naturwissenschaften* **2011**, *98*, 381–7, DOI: `10.1007/s00114-011-0781-4`.

(11) Gernay, S.; Federle, W.; Lambert, P.; Gilet, T. Elasto-capillarity in insect fibrillar adhesion. *J R Soc Interface* **2016**, *13*, DOI: `10.1098/rsif.2016.0371`.

(12) Ditsche, P.; Summers, A. P. Aquatic versus terrestrial attachment: Water makes a difference. *Beilstein Journal of Nanotechnology* **2014**, *5*, 2424–2439, DOI: `10.3762/bjnano.5.252`.

(13) Stark, A. Y.; Badge, I.; Wucinich, N. A.; Sullivan, T. W.; Niewiarowski, P. H.; Dhinojwala, A. Surface wettability plays a significant role in gecko adhesion underwater. *Proc Natl Acad Sci U S A* **2013**, *110*, 6340–5, DOI: `10.1073/pnas.1219317110`.

(14) Stark, A. Y.; Dryden, D. M.; Olderman, J.; Peterson, K. A.; Niewiarowski, P. H.; French, R. H.; Dhinojwala, A. Adhesive interactions of geckos with wet and dry fluoropolymer substrates. *Journal of The Royal Society Interface* **2015**, *12*, 20150464, DOI: `doi:10.1098/rsif.2015.0464`.

(15) Hosoda, N.; Gorb, S. N. Underwater locomotion in a terrestrial beetle: combination of surface de-wetting and capillary forces. *Proc Biol Sci* **2012**, *279*, 4236–42, DOI: `10.1098/rspb.2012.1297`.

(16) Brakke, K. A. The surface evolver. *Experiment. Math.* **1992**, *1*, 141–165.

(17) De Souza, E. J.; Brinkmann, M.; Mohrdieck, C.; Arzt, E. Enhancement of Capillary Forces by Multiple Liquid Bridges. *Langmuir* **2008**, *24*, 8813–8820, DOI: `10.1021/la8005376`.

(18) Arzt, E.; Gorb, S.; Spolenak, R. From micro to nano contacts in biological attachment devices. *Proc Natl Acad Sci U S A* **2003**, *100*, 10603–6, DOI: `10.1073/pnas.1534701100`.

(19) Sudersan, P. Buggee - An intergrative tool for synchronous data analysis, image processing and plotting. **2020**, DOI: `https://github.com/PranavSudersan/VScope`.

(20) Stark, A. Y.; Yanoviak, S. P. Adhesion and running speed of a tropical arboreal ant (Cephalotes atratus) on wet substrates. *Royal Society open science* **2018**, *5*, 181540–181540, DOI: `10.1098/rsos.181540`.

(21) Hsu, P. Y.; Ge, L.; Li, X.; Stark, A. Y.; Wesdemiotis, C.; Niewiarowski, P. H.; Dhinojwala, A. Direct evidence of phospholipids in gecko footprints and spatula - substrate contact interface detected using surface-sensitive spectroscopy. *Journal of The Royal Society Interface* **2012**, *9*, 657–664, DOI: `doi:10.1098/rsif.2011.0370`.

(22) England, M. W.; Sato, T.; Yagihashi, M.; Hozumi, A.; Gorb, S. N.; Gorb, E. V. Surface roughness rather than surface chemistry essentially affects insect adhesion. *Beilstein journal of nanotechnology* **2016**, *7*, 1471–1479, DOI: `10.3762/bjnano.7.139`.